Mon. Not. R. Astron. Soc. **359,** 455–463 (2005) doi:10.1111/j.1365-2966.2005.08958.x

A *Chandra* view of the anomalous half-merger NGC 520

Andrew M. Read★
Department of Physics and Astronomy, Leicester University, Leicester LE1 7RH

Accepted 2005 February 22. Received 2005 February 11; in original form 2004 September 20

ABSTRACT

High spatial and spectral resolution *Chandra* X-ray observations of the anomalous merging galaxy NGC 520, a similarly evolved system to the well-known Antennae galaxies, are presented here. Of great interest is the fact that NGC 520, on account of it being supposedly due (as seen in various multiwavelength studies) to the result of an encounter between one gas-rich disc and one gas-poor disc, appears in X-rays to be only 'half a merger'; whereas an ultraluminous X-ray source (ULX) lies at the primary (south-eastern), more-massive nucleus, no sources are seen at the secondary nucleus. Whereas what appears to be a starburst-driven galactic wind is seen outflowing perpendicular to the molecular disc surrounding the primary nucleus, no such diffuse structure is seen anywhere near the secondary nucleus. Comparing the X-ray properties with those of other merging galaxies, including famous gas-rich–gas-rich mergers such as the Mice and the Antennae, one sees that, relative to its star formation rate, the number of ULXs seen within the system is rather small. Similarly, the total X-ray luminosity and the fraction of this emission that appears diffuse are both a factor of $\sim$2 less than that expected based on NGC 520's evolutionary merger stage.

Although only half of NGC 520 appears in X-rays as other mergers do, there is still a wealth of structure and detail: 15 X-ray sources are detected within the system, many of them showing long-term variability, including a small number of bright ULXs that flatten the source X-ray luminosity function to a level similar to that of the Antennae and other mergers. Lastly, to see what appears to be a starburst-driven diffuse galactic wind, with a spectrum entirely consistent with that of other known galactic winds, although unusually, emanating from only one of the nuclei, is a surprise, given that one might have expected such structures to have distorted very quickly in such a rapidly evolving environment. The wind is larger and more massive than structures seen in evolutionarily earlier systems (e.g. the Mice), but smaller and less massive than as seen in later systems (e.g. the Antennae) or classic starbursts. Perhaps these structures can survive for longer than was previously thought.

Key words: ISM: jets and outflows – galaxies: haloes – galaxies: individual: NGC 520 – galaxies: ISM – galaxies: starburst – X-rays: galaxies.

1 INTRODUCTION

Merging and interacting are key elements in the life of galaxies, and underpin most current theories of galaxy formation and evolution. There are probably very few galaxies today that were not shaped by interactions or even outright mergers. Many mergers appear luminous in all wavebands. A very intense ($L_{\rm bol} > 10^{12}\,{\rm L}_{\odot}$) and spatially extended burst of star formation occurs in the evolution of most mergers. The hypothesis of Toomre (1977), whereby elliptical galaxies might be formed from the merger of two disc galaxies, is now generally accepted, such behaviour having been modelled in many N-body simulations of mergers (e.g. Toomre & Toomre 1972; Barnes 1988). During such an encounter, the conversion of orbital to internal energy causes the two progenitor discs to sink together and coalesce violently into a centrally condensed system. The 'Toomre sequence' (Toomre 1977) represents probably the best examples of nearby ongoing mergers, from disc–disc systems to near-elliptical remnants.

NGC 520 (Arp 157), the 'second brightest very disturbed galaxy in the sky' (Arp & Madore 1987) lies seventh in the Toomre sequence, and is classified as an intermediate-stage merger by Hibbard & van Gorkom (1996). It is as radio and infrared bright as the famous merging system, the Antennae, and has two smaller tails as well as two nuclei and two velocity systems in its spectra, indicative of a young merger. Some properties of the system are given

★E-mail: amr30@star.le.ac.uk

Table 1. Selected properties of NGC 520. Distance and optical luminosity L_B are taken from Tully (1988). Far-infrared luminosity is calculated from *IRAS* 60- and 100-μm fluxes, S_{60} and S_{100} (taken from the *IRAS* Point Source Catalogue), using the expression $L_{\rm FIR} = 3.65 \times 10^5 [2.58\ S_{60\,\mu{\rm m}} + S_{100\,\mu{\rm m}}]\ D^2\,{\rm L}_\odot$ (e.g. Devereux & Eales 1989). Radio luminosity is taken from Condon et al. (1990).

System	Other names	Distance (Mpc)	log L_B (erg s^{-1})	log $L_{\rm FIR}$ (erg s^{-1})	$L_{\rm FIR}/L_B$	S_{60}/S_{100}	log $L_{\rm rad}$ (W Hz^{-1})
NGC 520	Arp 157	28	43.87	44.15	1.900	0.651	22.24

in Table 1. A distance to NGC 520 of 28 Mpc is assumed in this paper (Tully 1988; Read & Ponman 1998, hereafter RP98); hence, 1 arcmin corresponds to ∼8 kpc. A brief introduction to the system is given below, and the previous X-ray observations are described in Section 1.1.

The nature of the peculiar system NGC 520 was once a puzzle; is it one disturbed galaxy or two interacting galaxies? Stanford & Balcells (1990) detected two galactic nuclei, just visible in the optical but more clearly in the *K* band. The less massive, secondary component (by perhaps more than an order of magnitude) is the north-western (NW) knot, which is optically brighter than the main [primary; south-eastern (SE)] component. The main component is optically weak because it is seen edge-on, and the light from its central region is absorbed by interstellar dust in its disc (visible as a dark lane in fig. 1 of Bernlöhr 1993). Furthermore, two hypotheses, either that the nearby dwarf galaxy UGC 957 might be primarily responsible for the disturbed morphology of a single galaxy in NGC 520, or that two interacting disc systems formed NGC 520, were tested with numerical simulations (Stanford & Balcells 1991). The simulations indicate that NGC 520 contains two interacting discs which collided $\sim 3 \times 10^8$ yr ago (UGC 957 was only involved in the producing of the northern half of a tidal tail).

Tovmasyan & Sramek (1976) found that the compact radio source in NGC 520 is situated in the dark lane between the two visible parts of the system. Condon et al. (1982) later resolved this into a 6-arcsec extension, consistent with an edge-on disc, lying almost east–west. More recent subarcsec angular resolution observations of the neutral gas and of the radio continuum structure at 1.4 and 1.6 GHz (Beswick et al. 2003) show this 6-arcsec feature to be made up of ∼10–15 individual clumps. Further, none of the clumps is found to have a radio spectral index compatible with active galactic nuclei (AGNs), and hence the most probable source of the radio emission is a nuclear starburst.

Millimetre-wave interferometer maps of the 2.6-μm CO emission (Sanders et al. 1988) show a strong peak at the position of this radio source; approximately $1.9 \times 10^9\ {\rm M}_\odot$ of molecular gas is concentrated in a region approximately 0.8 kpc in size. More recently, Yun & Hibbard (2001) have mapped the CO $J = 1 \rightarrow 0$ emission, and this is seen to form an east–west ring-like structure coincident with the radio structure. No molecular gas is seen near the NW nucleus, or indeed elsewhere in the system, and Yun & Hibbard suggest that the progenitor disc surrounding the secondary nucleus was rather gas-poor.

Much of the extranuclear regions of both galaxies within NGC 520 experienced a period of enhanced star formation $\sim 3 \times 10^8$ yr ago. The main-sequence remnants of this burst are the A stars whose features are evident in the optical spectra (Stanford 1991). The putative burst within the less massive NW nucleus has returned to a nominal level. The more massive, optically hidden SE nucleus produces stars at a rate of $\sim 0.7\ {\rm M}_\odot\ {\rm yr}^{-1}$ and is the current dominant source of star formation in this system. The star formation rate (SFR) within this region is ∼35 times higher than for an isolated disc galaxy. This region dominates the mid-infrared flux of the system, and probably produces most of the far-infrared flux seen in NGC 520.

The X-ray observations of NGC 520 prior to *Chandra* are described in the following subsection. Section 2 describes the *Chandra* observations and the data reduction techniques used. A discussion of the spatial, spectral and temporal properties of the source and diffuse emission components follows in Section 3, and in Section 4 the conclusions are presented.

1.1 Previous X-ray observations

NGC 520 has only previously been observed in X-rays with *ROSAT*, and the Position Sensitive Proportional Counter (PSPC) and High Resolution Imager (HRI) data were presented in RP98. The one PSPC source detected in the vicinity of NGC 520 at $\alpha = 01^{\rm h}24^{\rm m}34\overset{\rm s}{.}76$, $\delta = +03^\circ 47' 39\overset{''}{.}7$, lies within ∼5 arcsec of the radio source resolved by Condon et al. (1982), and is coincident with the more massive (the SE) of the two nuclei, as visible in the *K*-band image of Stanford & Balcells (1990). No source was detected at the position of the secondary NW nucleus.

NGC 520 appeared to be a very compact X-ray source with (very unusually for this type of system, and considering how infrared bright it is) little in the way of diffuse emission; a comparison of the radial emission profile with the *ROSAT* PSPC point spread function (PSF) indicated very little emission beyond 0.6 arcmin. The PSPC emission is almost consistent with point-source emission, and what diffuse emission exists, only makes up a very small fraction of the total. Little could be said about the spectral properties of the diffuse emission, except that it appeared soft.

The HRI image (RP98) showed more detail, and three sources were detected, the most northerly centred less than 5 arcsec east of the secondary (optically brighter) nucleus. This source, apparently associated with the NW nucleus, appears to be the hardest of the sources. A suggested extension to the east was also observed. The two other HRI sources both appear to be soft and they follow the bright band of optical emission down the NE side of the system.

2 *CHANDRA* OBSERVATIONS, DATA REDUCTION AND RESULTS

NGC 520 was observed with *Chandra* on 2003 January 29 for a total of just over 41 ks, with the back-illuminated ACIS-S3 CCD chip at the focus (observation ID 2924). Data products, correcting for the motion of the spacecraft and applying instrument calibrations, were produced using the Standard Data Processing (SDP) system at the *Chandra* X-ray Center (CXC). These products were then analysed using the CXC CIAO software suite (version 3.0).

A light curve extracted from a large area over the entire observation was seen to be essentially constant and consistent with a

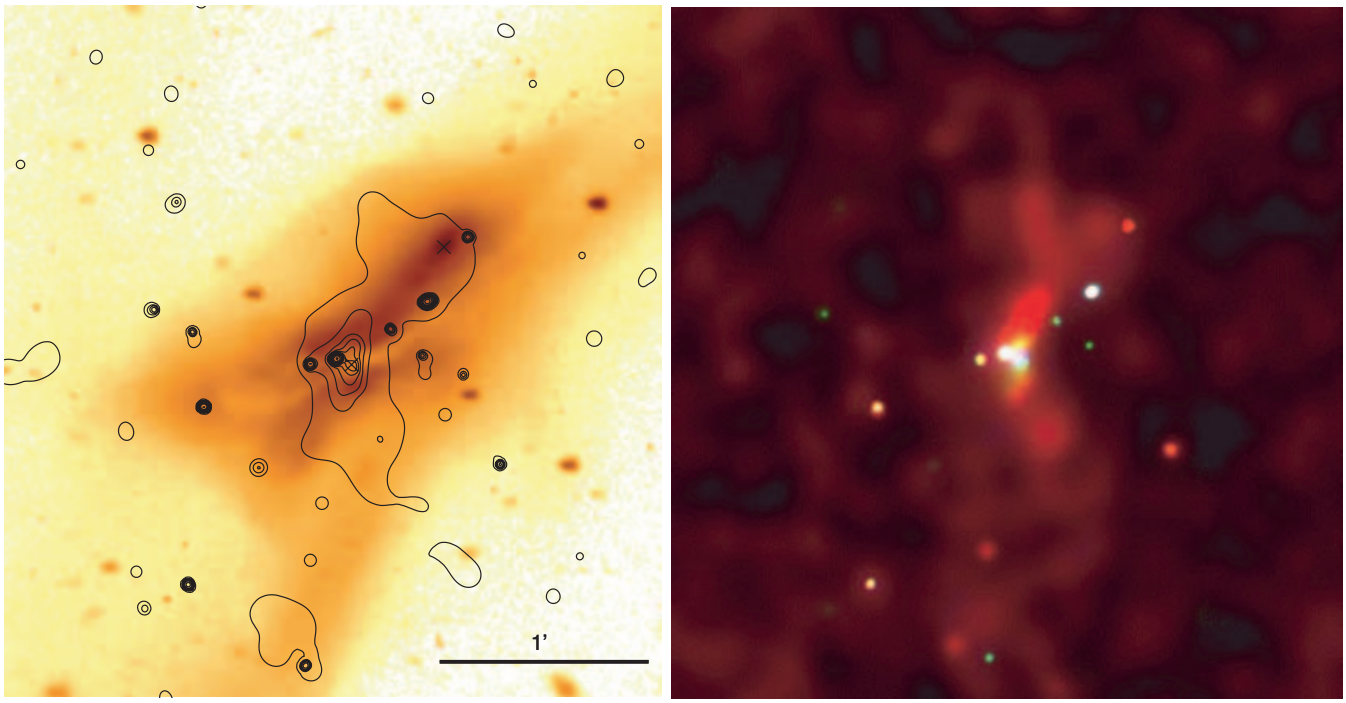

Figure 1. Left: contours of adaptively smoothed (0.2–10 keV) *Chandra* ACIS-S X-ray emission from the field surrounding NGC 520, superimposed on the *V*-band KPNO 0.9-m image from Hibbard & van Gorkom (1996). The X-ray contours increase by factors of 2. The crosses mark the positions of the two nuclei (from Stanford 1991). Right: 'true colour' X-ray image of NGC 520 to the same scale. Red corresponds to 0.2–0.9 keV, green to 0.9–2.5 keV and blue to 2.5–10 keV. For scale, the images are approximately 3 arcmin to a side.

low-level rate, apart from a couple of high-background peaks. Screening of the data to remove these periods (at a level of 2.44 ct s^{-1} $arcmin^{-2}$) was performed.

2.1 Overall X-ray structure

Fig. 1 (left) shows contours of adaptively smoothed (0.2–10 keV) *Chandra* ACIS-S X-ray emission from the field surrounding NGC 520, superimposed on the *V*-band Kitt Peak National Observatory (KPNO) 0.9-m image from Hibbard & van Gorkom (1996). Note that the secondary (NW), less massive nucleus is quite visible in the optical image, whereas the primary (SE) nucleus is hidden by the obscuring dust lane. The adaptive smoothing of the X-ray emission attempts to adjust the smoothing kernel to obtain a constant signal-to-noise ratio across the image.

Several things are immediately evident from the image. Many bright point sources are visible within the optical confines of the system. Residual, perhaps diffuse, emission is seen concentrated and centred in the dust lane at the centre of the galaxy, but extending initially in a general north–south direction, and also following slightly the general shape of the galaxy to the north-west.

Fig. 1 (right) shows a true colour X-ray image, with red corresponding to 0.2–0.9 keV, green to 0.9–2.5 keV and blue to 2.5–10 keV. The individual adaptively smoothed images were obtained as described above. The image is to the same scale as Fig. 1 (left), and all the X-ray features are visible. A large range in spectral hardness is seen within the point sources, and the residual, perhaps diffuse, emission is seen to be very much softer than the point-source emission.

2.2 Point sources: spatial and spectral properties

The CIAO tool WAVDETECT was used to search for point-like sources, on scales from 1 to 16 pixels (0.5–8 arcsec). A total of 15 sources were detected in the 0.2–7.5 keV band within or close to the optical confines of the galaxies, and their X-ray properties are summarized in Table 2. Fig. 2 shows the positions of the detected sources.

The X-ray properties given in Table 2 are as follows. Right ascension and declination (2000.0) are given in columns 2 and 3, together with (column 4) the positional error (in arcsec), calculated from the WAVDETECT errors in RA and Dec. (no corrections on the absolute astrometry have been applied). Net source counts (plus errors, both from CIAO WAVDETECT) are given in column 5, and the source significance is given in column 6. Columns 7 and 8 give the fitted hydrogen column and power-law photon index (an 'F' indicating that the parameter was frozen (see below for a discussion of the spectral fitting). For those fits where a significant number of degrees of freedom existed (>1; see below), this is given, together with the best-fitting χ^2 in column 9. Finally, (0.2–10 keV) X-ray emitted and intrinsic (i.e. corrected for absorption) luminosities are given in columns 10 and 11.

Source spectra were extracted at the exact positions given by the 0.2–7.5 keV detection analysis. The regions output by the detection routines were invariably near-circles of radius $\lesssim$8 pixels (partly due to NGC 520 only occupying the very centre of the ACIS-S3 chip). Consequently, a single extraction radius of 8 pixels (4 arcsec) was defined and used for all the sources in Table 1. A large area to the SW of the system, chosen close enough to the system to minimize effects related to the spatial variations of the CCD response, but free of source and apparent diffuse emission, was chosen to construct a background spectrum.

ACIS spectra were extracted using pulse invariant (PI) data values, and were binned together to give a minimum of 10 counts per bin after background subtraction. Hence, χ^2 statistics could be used. Response matrices and ancillary response matrices were created for each spectrum, using the latest calibration files available at the time of writing.

Table 2. Sources detected by WAVDETECT in the 0.2–7.5 keV band within or close to the optical confines of NGC 520. Columns are described in the text. Luminosities assume a $\Gamma = 1.5$ photon index power law plus Galactic absorption, except for sources 9, 11, 12 and 15, where the spectral parameters are given. A distance of 28 Mpc has also been assumed.

Src.	RA (2000.0)	Dec. (2000.0)	Pos. err. (arcsec)	Counts (err)	Sig.	$N_{\rm H}$ 10^{20} cm^{-2}	Photon Index Γ	χ^2 ($N_{\rm dof}$)	$L_{\rm X}$ (0.2–10 keV) (10^{39} erg s^{-1}) (emitted)	(intrinsic)
7	01 24 37.82	+03 46 25.9	0.11	34.7± 6.0	14.2	3.27(F)	1.5(F)	–	0.75	0.77
8	01 24 37.67	+03 47 16.1	0.08	48.2± 7.1	18.5	3.27(F)	1.5(F)	–	0.92	0.95
9	01 24 35.68	+03 47 29.7	0.14	56.0± 8.0	14.1	$108^{+77.8}_{-22.9}$	$3.5^{+0.6}_{-0.8}$	2.7(3)	0.80	4.38
10	01 24 35.50	+03 46 04.9	0.22	22.4± 5.0	7.9	3.27(F)	1.5(F)	–	0.74	0.75
11	01 24 35.19	+03 47 31.4	0.24	874.9±30.5	103.2	$40.0^{+3.9}_{-3.5}$	$2.4^{+0.1}_{-0.1}$	74.5(73)	15.89	34.97
12	01 24 34.89	+03 47 29.5	0.13	111.6±13.2	12.5	$48.4^{+45.0}_{-21.3}$	$1.1^{+0.4}_{-0.2}$	40.4(20)	8.89	10.13
13	01 24 34.19	+03 47 40.4	0.23	21.9± 5.1	6.8	3.27(F)	1.5(F)	–	0.60	0.61
14	01 24 33.53	+03 47 33.4	0.32	11.9± 3.7	4.4	3.27(F)	1.5(F)	–	0.23	0.25
15	01 24 33.50	+03 47 48.8	0.05	354.0±19.2	75.1	$44.5^{+13.7}_{-9.9}$	$1.8^{+0.1}_{-0.1}$	23.1(30)	10.00	13.45
18	01 24 32.79	+03 48 07.4	0.16	21.0± 4.8	7.8	3.27(F)	1.5(F)	–	0.29	0.30
19	01 24 32.73	+03 47 29.1	0.35	8.8± 3.2	3.6	3.27(F)	1.5(F)	–	0.21	0.22
20	01 24 31.96	+03 47 04.4	0.28	15.1± 4.2	5.2	3.27(F)	1.5(F)	–	0.36	0.36
23	01 24 40.23	+03 45 50.0	0.35	12.0± 3.9	4.1	3.27(F)	1.5(F)	–	0.17	0.17
25	01 24 37.99	+03 47 36.9	0.32	9.2± 3.3	3.5	3.27(F)	1.5(F)	–	0.34	0.34
26	01 24 36.60	+03 46 59.9	0.31	8.0± 3.0	3.4	3.27(F)	1.5(F)	–	0.20	0.22

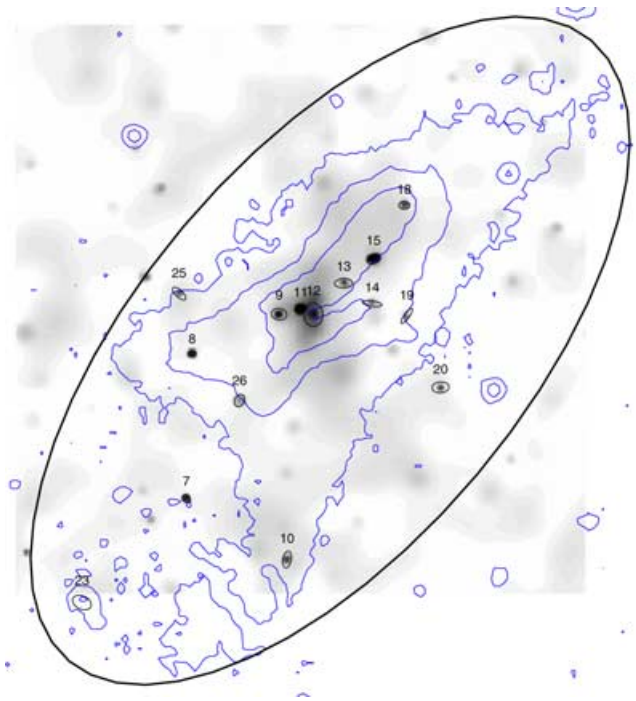

Figure 2. Adaptively smoothed (0.2–10 keV) ACIS-S image labelled with sources detected in the 0.2–7.5 keV band. The large ellipse shows the area over which the diffuse emission spectrum was extracted, and the contours (blue in the online version of the article) show schematically the optical confines of the system (see Fig. 1).

Standard spectral models were fit to the spectral data using the XSPEC spectral fitting software. Events above 7.5 keV (of which there were very few) and below 0.25 keV were excluded from the fitting on the grounds of uncertainties in the energy calibration. It is now known that there has been a continuous degradation in the ACIS QE since launch. A number of methods now exist within the community to correct for this. These include the release of an XSPEC model (ACISABS) to account for this degradation, and the existence of software (CORRARF) to correct the ancillary response files. The analysis performed in the present paper has made use of CALDB v2.23, which does not include a correction for the ACIS QE degradation. Hence, both the above methods have been used here in the spectral fitting, and very similar results were obtained. In both cases, the time since launch of the observations (here, 1286 d) is used in the correction. Although the calibration at energies below 1.0 keV is believed to be uncertain, data in this range were kept, as the statistical error on these data points is still greater than the errors due to the uncertainties in the calibration.

Two models were fit to the source data: one incorporating absorption fixed at the value out of our Galaxy (3.27×10^{20} cm^{-2}) and a 5-keV MEKAL thermal plasma, and the other incorporating absorption (again, fixed) and a power law of photon index 1.5. For the majority of the sources, there were insufficient counts to allow the model parameters to vary, but for sources 9, 11, 12 and 15, there were sufficient counts (>50) to allow the model parameters to fit freely.

For three of these four cases (9, 11 and 15), F-tests showed that statistically significant improvements in the fits were made on freeing the parameters. Also, in these three cases, better fits (with reduced $\chi^2 < 1$) were obtained using a power-law model over a thermal model, and these model parameters are quoted in Table 2. The fit to source 12 is not too good (with a reduced χ^2 of $\approx$2), and this is discussed further in Section 3.1.

The luminosities quoted in Table 2 for sources 9, 11, 12 and 15 assume these best-fitting models, while for the other sources, the model assumed is of a fixed (Galactic) absorption plus a power law of photon index 1.5.

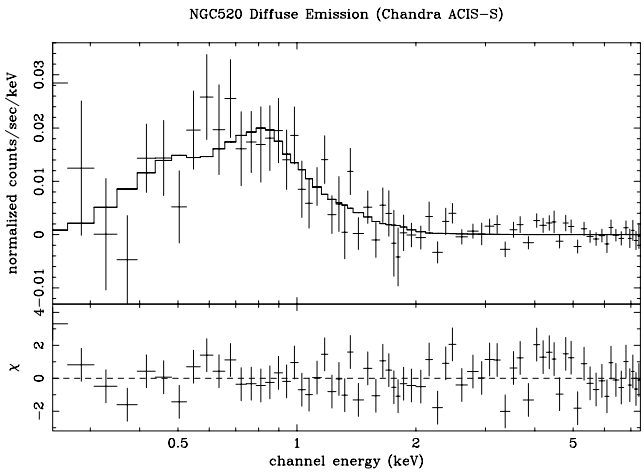

Figure 3. Data (points) plus best-fitting thermal MEKAL model (lines) for the residual emission within NGC 520. The lower panel shows the (data–model) $\Delta\chi^2$ values.

2.3 Residual emission: spatial and spectral properties

The existence of residual, likely diffuse, emission is very evident in the figures. A spectrum from this region of apparent diffuse emission was extracted – the ellipse in Fig. 3 shows the area over which the spectrum was extracted, with the sources also excluded to a radius of 4 arcsec. Again the spectral channels were binned together to give a minimum of 10 counts per bin.

The spectral fitting was performed as for the point sources, using the same models, and using both methods to correct for the degradation in the ACIS QE. While an absorption plus power-law model was unable to fit the data satisfactorily, a thermal model proved much better, and the best thermal fit (using an absorption plus MEKAL model) is summarized in Table 3; the absorbing column, the fitted temperature and metallicity, the reduced χ^2, and the emitted and intrinsic (i.e. total $N_{\rm H}$ absorption-corrected) X-ray luminosity are given. The data plus best-fitting model is shown in Fig. 3. A reanalysis of the data using a grouping of 20 counts per bin gave essentially identical results to those given here.

3 DISCUSSION

3.1 Point sources

Within the general optical confines of NGC 520 (i.e. within the ellipse shown in Fig. 2), 15 sources are detected with the *Chandra* ACIS-S instrument, down to a (0.2–10.0 keV) detection limit of $\approx 1.7 \times 10^{38}$ erg s^{-1}. Previous detections of X-ray sources include the one source (P1) detected with the *ROSAT* PSPC, and the three sources (H1–H3) detected by the *ROSAT* HRI (RP98). One can use the log N–log S relations of Rosati et al. (2002) to estimate the expected number of background sources not physically associated with NGC 520. At most, perhaps two background sources are expected over the ellipse covered by Fig. 2 at the detection limit seen here.

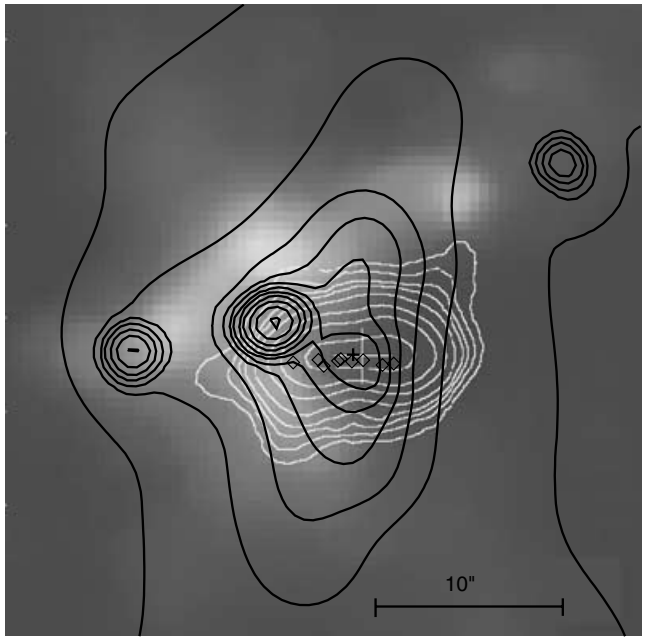

Figure 4. The central region of NGC 520. Black contours show the contours of adaptively smoothed (0.2–10 keV) *Chandra* ACIS-S X-ray emission (from Fig. 1, left). White contours show the velocity-integrated CO(1–0) map of Yun & Hibbard (2001). The small black cross shows the position of the primary nucleus from Stanford (1991). The large white cross shows the centre of the 6-arcsec radio source of Condon et al. (1982), and the diamonds show the positions of the nine main 1.4-GHz components resolved within the 6-arcsec Condon feature by Beswick et al. (2003). The underlying grey-scale shows the Hα image emission from Yun & Hibbard (2001). The image is $\approx$33 arcsec across.

Source 12 is bright (although only the third brightest source), spectrally quite hard (as indicated by the blue–white appearance in the RGB plot; Fig. 1, right), and is coincident (<0.5 arcsec) with the primary nucleus, i.e. the Condon et al. (1982) radio source and the Yun & Hibbard (2001) CO feature. It lies at the centre of the brightest part of the much softer diffuse X-ray emission (discussed in the next subsection). The central region of NGC 520 is shown more clearly in Fig. 4, where the adaptively smoothed (0.2–10 keV) *Chandra* ACIS-S X-ray emission (from Fig. 1, left), the velocity-integrated CO(1–0) map of Yun & Hibbard (2001), the Hα emission from Yun & Hibbard (2001), the Stanford (1991) primary nucleus position, the Condon et al. (1982) 6-arcsec radio source and the positions of the main 1.4-GHz components resolved within the 6-arcsec Condon feature by Beswick et al. (2003) are all shown together. In actuality, *Chandra* source 12 lies closest to (<0.2 arcsec) the brightest and most central of the Beswick et al. (2003) radio features (their feature 6). Taking also into account uncertainties in *Chandra*'s

Table 3. Best results of fitting a thermal model to the spectrum of the residual emission within NGC 520. Luminosities assume a distance of 28 Mpc (see text).

Diff. src.	Counts (err)	$N_{\rm H}$ (10^{20} cm^{-2})	kT (keV)	Z (solar)	χ^2 (red.)	L_X (0.2–10 keV) (10^{39} erg s^{-1}) (emitted)	(intrinsic)
NGC 520	896.8 ± 112.6	3.27(F)	$0.58^{+0.09}_{-0.11}$	<0.04	0.95	6.40	8.03

absolute astrometry (≈0.7 arcsec for on-axis, isolated point sources), then the *Chandra* source 12 error circle could also just encompass radio feature 7 (the second brightest feature of Beswick et al. 2003). *Chandra* source 12 is undoubtedly associated with the primary nucleus of NGC 520. A spectral fit to the spectrum of source 12, but using a model incorporating an extra component to represent the soft, thermal diffuse emission (with fixed parameters as given in Table 3), results in a far better fit to the source 12 data (with a reduction in reduced χ^2 of $\gtrsim$0.5). An F-test shows this improvement to be statistically significant at over 97 per cent confidence. Here, the hard component (assumed due to the actual source 12 itself) is better represented by a power-law model ($N_{\rm H} = 2.3 \times 10^{22}$ cm^{-2}, $\Gamma = 2.15$) than a thermal model ($N_{\rm H} = 2.5 \times 10^{22}$ cm^{-2}, $kT =$ 3.1 keV). In both cases, the hard (i.e. the point source) component makes up ≈90 per cent of the total emitted (0.2–10 keV) flux from source 12.

Source 11 is the brightest of the X-ray sources and lies at the easternmost edge of the radio/CO disc. Although it could be enclosed within the *ROSAT* H3 and H2/P1 sources and the complex and confused PSPC/HRI emission surrounding the primary nucleus, this appears not too likely. Source 15, the second brightest source, does not have a direct counterpart in the HRI (or the relatively poor positional resolution PSPC) observations, and this would indicate that source 15 (and likely source 11) are transient in nature. Both sources are well fit with single-component power-law models (Table 2).

Sources 8 and 9 are both fairly bright and fairly soft/medium-temperature sources. Source 9 is associated with H3, and source 8 may have a low-significance HRI counterpart. Of the remaining, lower-luminosity sources, source 18 lies closest to the secondary (NW) nucleus (visible in the *V*-band image of Fig. 1, left), but still lies some 7 arcsec distant; hence, interestingly, no X-ray emission is coincident with the secondary nucleus, and the HRI source (H1) tentatively associated (RP98) with the NW nucleus appears to have vanished. Given the astrometric uncertainties in the *ROSAT* position it is unlikely that source 8 is coincident with H1.

Beswick et al. (2003) believe that two different components of gas (neutral gas and ionized gas), with very different velocity characteristics, can be sampled within NGC 520, and these components are located at different distances from the primary nucleus. Whereas the velocity structure of the neutral ISM components within the central regions of the primary nucleus (Fig. 4) are probably more characteristic of the rotational motion of the progenitor galaxy nucleus, the very different velocities observed (e.g. Stockton & Bertola 1980; Bernlöhr 1993) for the ionized gas located a few kpc from the primary nucleus have likely been imparted on the gas by the merger event. It is very interesting to note that there are many bright sources (notably 9, 11 and 13) that lie in this zone where the two velocity systems are colliding, a region where strong shocks and large compressions of gas are expected to occur. Indeed, the Hα emission (Yun & Hibbard 2001) indicates that a good deal of star formation is certainly taking place on the eastern side of the zone where the two velocity systems are colliding, in the region occupied by sources 9 and 11.

The cumulative X-ray luminosity function (XLF) of the sources detected within NGC 520 is shown in Fig. 5. Plotted is the (log of the) number of sources above a given X-ray luminosity versus the (log of the) X-ray luminosity. The functions for the intrinsic and emitted values (see Table 2) are given. While simple regression fitting of a linear function to log N against log $L_{\rm X}$ leads to a slope of 0.45 (usage of the emitted $L_{\rm X}$ values leads to a slope of 0.50), a more appropriate approach, and one where the errors of the Poissonian statistics of the data are better reflected, is to fit the differential luminosity

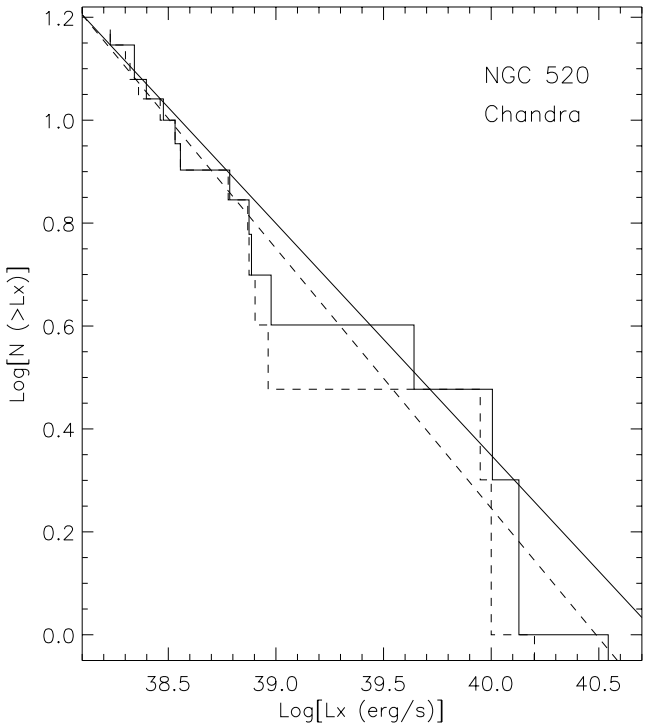

Figure 5. The cumulative luminosity function of the discrete sources detected within NGC 520. Plotted is the log of the number of sources above a given X-ray luminosity versus (log of the) X-ray luminosity. The functions for the intrinsic (solid line) and emitted (dashed line) values (see Table 2) are given. The straight solid and dashed lines show the best regression fits to the two functions (see text).

function, using the method of Crawford, Jauncey & Murdoch (1970). This gives more realistic errors on the fitted slope. Use of this method gives slopes of 0.58 ± 0.15 for the intrinsic $L_{\rm X}$ values (and 0.66 ± 0.17 for the emitted $L_{\rm X}$ values).

Colbert et al. (2004) have found that, while ellipticals have very steep XLF slopes (-1.41 ± 0.38), the slopes for spirals are much flatter (-0.79 ± 0.24), and for merging galaxies and irregular galaxies, the slope is even flatter still (-0.65 ± 0.16). NGC 520 therefore has a very flat XLF, consistent with it being a highly irregular, merging galaxy. NGC 520 in fact has an XLF slope similar to that of the Antennae (-0.47 ± 0.05; Zezas & Fabbiano 2002), a system with a very similar far-infrared luminosity, and a system at a similar to slightly later evolutionary stage.

The number of ultraluminous X-ray sources (ULXs), i.e. sources with $L_{\rm X} \gtrsim 10^{39}$ erg s^{-1}, in NGC 520 is around three to four (i.e. sources 11, 12 and 15, with possibly source 9). Were it not for these sources, the XLF would appear rather steeper than it does in Fig. 5, looking more like that of normal spirals. The three definite ULXs, in fact, make up most of the total X-ray flux, accounting for 85 per cent of the point-source emission, and 73 per cent of the total emission.

There is evidence to suggest that galaxies with a greater SFR contain a greater number of ULXs (Swartz et al. 2004), and it is these sources that flatten the XLF. Brassington, Read & Ponman (2005) have presented a relationship between the number of ULXs and the far-infrared luminosity for a small number of interacting and merging galaxies: log N(ULX) $\propto$ log $L_{\rm FIR}^{0.18\pm0.13}$. NGC 520 appears unusual in that it does not fit into this picture at all, having a large $L_{\rm FIR}$ value, very like that of, for example, the Mice or the Antennae, but a relatively small number of ULXs (three to four). Based on the

number of ULXs per unit far-infrared luminosity, one would expect there to be about 10 ULXs in NGC 520, if it were similar to the Antennae.

Furthermore, Brassington et al. (2005) observe a relationship between the integrated luminosity of the ULX sources and the far-infrared luminosity in their merging galaxy sample: $\log L_{\rm ULX} \propto \log L_{\rm FIR}^{0.54\pm0.04}$. The small number of NGC 520 ULXs are all bright, but, even so, NGC 520 lies significantly below the observed $L_{\rm ULX}$–$L_{\rm FIR}$ relationship.

3.2 Diffuse emission

The residual emission, given its structure and its spectrally soft, single-component nature, is very likely predominantly due to genuinely diffuse hot (0.58 keV) gas (although there will be some contribution from unresolved sources).

It appears centred on *Chandra* source 12, at the precise site of the primary, more massive, optically obscured nucleus, a nucleus believed not to harbour any AGNs, but believed to be a starburst-powered nucleus (Beswick et al. 2003). The diffuse emission is seen to extend in a bipolar form initially to the north and to the south, i.e. directly perpendicular to the molecular disc (Yun & Hibbard 2001) surrounding the primary nucleus, a disc also observed in the radio (Condon et al. 1982; Beswick et al. 2003). This north–south extension is seen to be quite bright for quite a distance (∼2 kpc from the nucleus), and then becomes somewhat weaker, perhaps more so to the south, reaching a final extent of perhaps ∼7 kpc (to the north) and ∼5.5 kpc (to the south). It is quite unlikely that the north–south extension could be predominantly due to absorption by cold disc gas, as the CO gas exists in only a small (∼12 arcsec) centralized region, and the rather diffuse neutral H I gas (Yun & Hibbard 2001) pervades much of the system, and extends in a more SE–NW direction, in a direction roughly connecting the two nuclei. It is very interesting to note that there appears to be no significant enhancement in the diffuse emission, nor in the X-ray emission in general, in the vicinity of the secondary nucleus.

All these points, both spatial and spectral, are very suggestive of the diffuse structure being due predominantly to a small version of a starburst-driven wind from solely the primary (SE) nucleus. Further evidence is suggested by the ionized Hα emission (visible in Fig. 4), following roughly the inner structure of the diffuse X-ray feature. Yun & Hibbard (2001) conclude that this Hα emission is likely dominated by the 'starburst-driven ionized wind' escaping to the north and south. Interestingly, there is no evidence whatsoever for any similar structure in the secondary (NW) nucleus. Classic winds, such as those seen in famous nearby starburst galaxies such as M82 and NGC 253 (e.g. Strickland et al. 2002; Stevens, Read & Bravo-Guerrero 2003) are rather isolated, and it is rather surprising to see what appears to be a bipolar wind in even one member of a strong, rapidly evolving interacting pair, such as here in NGC 520. It is believed (Read 2003) that the very beginning of starburst-driven hot gaseous outflows in full-blown disc–disc mergers has been seen in the Mice. One might have thought that later systems would have evolved to such a degree that any classic starburst wind or winds (were they to have existed) would have been distorted out of recognition. Indeed, *Chandra* observations of the Antennae (a system believed to be post-Mice, but more like at the evolutionary stage of NGC 520) show a great deal of hot diffuse gas, but it has become all-pervasive, extending beyond the stellar bodies of the galaxies (Fabbiano, Zezas & Murray 2001).

One can infer mean physical properties of the hot gas around the northern and southern galaxies once some assumptions have been made regarding the geometry of the diffuse emission. Two models have been used here. A conservative model assumes the gas here to be contained in an elliptical bubble [the ellipse as shown in Fig. 2 and the third (line-of-sight) axis assumed equal ('radius' 9.2 kpc) to the short axis of the ellipse]. A more stringent, and probably more realistic model, roughly follows the outer contours of the X-ray emission and assumes the gas to be contained in a spherical bubble of radius 45 arcsec (corresponding to 6.1 kpc). Using these volumes, the fitted emission measure $\eta\, n_{\rm e}^2 V$ (where η is the 'filling factor', the fraction of the total volume V that is occupied by the emitting gas) can be used to infer the mean electron density $n_{\rm e}$, hence assuming a plasma composition of hydrogen ions and electrons, the total mass $M_{\rm gas}$ and thermal energy of the gas $E_{\rm th}$. Approximate values of the cooling time $t_{\rm cool}$ of the hot gas, and also the mass cooling rate $\dot{M}_{\rm cool}$ can also be calculated. The resulting gas parameters for both models are listed in Table 4.

Comparing the diffuse gas parameters in Table 4 with those for isolated normal and starburst galaxies (Read, Ponman & Strickland 1997), and for merging galaxies (RP98; Fabbiano et al. 2001; Read 2003), one can say that the single diffuse outflow observed in NGC 520 is larger than the outflows seen in the earlier-stage Mice (2–3 kpc), but it is not as large as the classic winds of M82 and NGC 253 (9–14 kpc), nor quite as large as the outflowing, non-collimated turbulent interstellar medium (ISM) of the Antennae (≈8 kpc). There appears to be more diffuse gas within the NGC 520 system than in the Mice, but this gas mass, while possibly comparable to that of NGC 253 and of the order of half that seen in M82, is only 10–20 per cent of that seen in the Antennae.

The injection rate of mechanical energy, or power injected into a particular galaxy by supernovae, can be estimated by the method employed in Read & Ponman (1995), and this value for NGC 520 is seen to be very similar to that of the Antennae and M82. The amount of hot gas in NGC 520, expressed as a fraction of input energy therefore is rather small. Note that, as the diffuse gas has a very long cooling time, no significant fraction of the gas has had time to cool.

Although it is believed that the hot ISM of starburst galaxies has a multitemperature structure, the single temperature obtained from the spectral fitting of the diffuse spectrum (≈0.58 keV) is entirely consistent with the range obtained for other starburst and merging galaxies.

Table 4. Values of physical parameters for the diffuse gas associated with NGC 520. The values quoted are for a large ellipsoidal bubble model and a small spherical bubble model (see text). η is the filling factor of the gas.

Diff. model	kT (keV)	r (kpc)	$n_{\rm e}$ (cm^{-3}) ($\times 1/\sqrt{\eta}$)	$M_{\rm gas}$ (M$_\odot$) ($\times\sqrt{\eta}$)	$E_{\rm th}$ (erg) ($\times\sqrt{\eta}$)	$t_{\rm cool}$ (Myr) ($\times\sqrt{\eta}$)	$\dot{M}_{\rm cool}$ (M$_\odot$ yr^{-1})
Large ellipse	0.58	9.2	6.9×10^{-3}	7.1×10^{8}	1.9×10^{57}	7590	0.094
Small bubble	0.58	6.1	1.9×10^{-2}	2.8×10^{8}	7.6×10^{56}	3560	0.079

3.3 X-ray emission from NGC 520

NGC 520 is very far-infrared bright, and consequently has a large value of $L_{\rm FIR}/L_B$. It also has a large far-infrared temperature, S_{60}/S_{100}, and both these are indicative of NGC 520 having a high SFR and being very active, more active than the famous interacting systems, Mice and Antennae.

The total emitted 0.2–10 keV X-ray luminosity of NGC 520, assuming a distance of 28 Mpc, is 4.74×10^{40} erg s^{-1}, of which the diffuse emission makes up 13.5 per cent (the equivalent intrinsic absorption-corrected values are 7.64×10^{40} erg s^{-1} and $f_{\rm diff} = 10.5$ per cent).

The value of $L_{\rm X}$ quoted here may initially appear at odds with the low value ($\approx 1 \times 10^{40}$ erg s $-$ 1) given in RP98. There are a few points to note here. The energy bands over which the luminosities are calculated are different. The RP98 value is based on the results of spectrally fitting the PSPC data; this analysis was prone to difficulties and the spectral parameters obtained had large errors. In actuality, using PIMMS to predict the *Chandra* ACIS-S count rate, based purely on the HRI count rate, allowing for the different energy ranges, and using a much more appropriate spectral model (a $\Gamma = 1.5$ power law) does give a similar result to what we actually observe with the ACIS-S (to within 2 per cent). Lastly, there is quite evidently a lot of variability going on within the point sources, so we should expect some variation in $L_{\rm X}$ between the observations.

As such, the larger X-ray luminosity inferred here for NGC 520 indicates that it is not as anomalous as was first thought in RP98; both its position in the $L_{\rm X}$–$L_{\rm FIR}$ plane (RP98, fig. 14) and its position in the $L_{\rm X}/L_B$-versus-age plane (RP98, fig. 13) appear closer in line with the other similar-stage mergers than as depicted in RP98. However, while taking into account the points raised in the previous paragraph, NGC 520 still appears somewhat underluminous in X-rays, for its merger stage, perhaps by a factor of up to 2.

Yun & Hibbard (2001) discovered that, although a dense concentration of molecular gas is seen at the primary (SE) nucleus, none is seen at the secondary (NW) nucleus, nor along the region bridging the two nuclei. The Hibbard & van Gorkom (1996) analysis of the stellar and H I features in NGC 520 indicated that NGC 520 is the product of an encounter between a gas-rich disc and a gas-poor disc (e.g. an S0 and Sa galaxy). The absence here of molecular gas in the NW nucleus can be explained if little molecular gas had been compressed towards the nucleus during the merger process, there being little gas in the progenitor disc to start with. Similar analyses have concluded that systems such as the Mice and the Antennae are each the product of encounters between two gas-rich systems.

This initial lack of gas in the NW progenitor is a very likely explanation of several facets of the X-ray emission discussed here. The fact that there was no gas in the disc meant that no gas could be funnelled towards the NW nucleus during the interaction. Consequently, little in the way of a starburst could take place at the NW nucleus, and no collections of supernovae could collect and expand outwards in the form of a starburst-driven wind or of fountains or chimneys etc.; there would be, as is observed, no diffuse X-ray emission surrounding the NW nucleus. The percentage of the total X-ray emission in NGC 520 observed to be diffuse ($f_{\rm diff}$) is low ($\sim$13.5 per cent), when compared with roughly similar-stage systems (e.g. the Antennae, 45 per cent; Fabbiano et al. 2001), and even when compared with very early-stage interacting systems (e.g. Arp 270, 29 per cent; Brassington et al. 2005). Were the progenitor disc that formed the NW nucleus initially gas-rich, then $f_{\rm diff}$ for NGC 520 would certainly be larger (although not by a factor of 2), and perhaps more in line with other merging systems.

Further, as discussed earlier, the number of ULXs observed is very low when compared to other mergers. It is well known (e.g. Roberts et al. 2002) that ULXs are more prevalent in regions of enhanced star formation. If a starburst were to have occurred in the NW nucleus similar to that in the SE nucleus, then the number of ULXs within the NGC 520 system may well have been more like that of similar merger systems.

Lastly, the arguments raised here could increase the total X-ray luminosity, perhaps by the factor of $\sim$2 required, bringing NGC 520 more in line with its expected position in the X-ray evolution of merging galaxies.

4 CONCLUSIONS

Presented here are high spatial and spectral resolution *Chandra* ACIS-S X-ray observations of the interacting galaxy system, NGC 520, a system at a similar or slightly later evolutionary stage as the Antennae, i.e. more evolved than the Mice but not as evolved as the ultraluminous contact mergers, such as Arp 220. The primary results can be summarized as follows.

(i) What appears to be possibly a starburst-driven galactic wind has been discovered, outflowing perpendicular to the molecular disc surrounding the primary, optically obscured SE nucleus. No such structure, nor any significant diffuse feature of any kind, is visible elsewhere in the system, and it is notably absent from around the secondary NW nucleus. Fitting of this diffuse emission yields a temperature entirely consistent with well-known nearby galactic winds. In terms of extent and mass, the wind appears larger and more massive than the winds of earlier-stage mergers, but it is only at most of the order of the size and mass of the winds seen in the smaller nearby starbursts, and it is rather much smaller and less massive than the diffuse structure seen in, for example, the Antennae (a structure that appears more like a non-collimated outflow originating from the galaxy-wide star formation, rather than a galactic wind-type outflow). One might have expected the NGC 520 wind structures to distort very quickly, due to the rapid evolution and violence of the environment. However, the structure appears, especially towards the centre, to be rather classical in nature, and a single starburst-produced wind might indeed last intact for some time during a major interaction.

(ii) 15 X-ray sources are detected within the optical confines of the system. Of these, three or possibly four are ULXs, each with $L_{\rm X}$ (0.2–10 keV) $\gtrsim 10^{39}$ erg s^{-1}. One of the ULXs lies at the primary nucleus, at the centre of the diffuse wind structure, and coincident with the bright radio source at the centre of the molecular disc. A number of the other bright sources are seen to lie near the edge of this molecular disc, in an interface region between the progenitor-galaxy-driven centrally located neutral ISM and the merger-driven outlying ionized ISM. Significantly, no sources are detected at the secondary nucleus, although, within the system, much apparent point-source variability is seen between the observations described here and earlier *ROSAT* observations.

(iii) The slope of the source X-ray luminosity function (XLF) is very flat, due predominantly to the ULXs, and appears in sharp contrast to that of other normal and starburst galaxies. It is however similar to that of the Antennae and other merging galaxies.

(iv) There is much in the X-ray data to support the idea, as suggested by previous multiwavelength studies, that NGC 520 is the result of an encounter between one gas-rich disc and one gas-poor disc. The number of ULXs observed is only three to four, while one would expect, on the basis of the far-infrared luminosity, a

number closer to 10. Similarly, $L_{\rm ULX}$ is lower than would be expected, based on the $L_{\rm FIR}$ value. No sources are seen coincident with the secondary (NW) nucleus, nor is any diffuse emission observed in or around this nucleus. The total X-ray luminosity compared to other multiwavelength luminosities, and the diffuse gas fraction are down by about a factor of 2, based on what would be expected, given NGC 520's evolutionary merger stage. It does seem therefore that, in terms of the X-ray properties, because of the fact that NGC 520's progenitors are likely only one gas-rich disc plus one gas-poor disc, we are observing only 'half a merger' when compared with similar gas-rich–gas-rich merger systems, such as the Antennae and the Mice.

ACKNOWLEDGMENTS

AMR acknowledges the support of UK Particle Physics and Astronomy Research Council (PPARC) funding, and thanks the referee (A. Zezas) for very useful comments which have helped to improve the paper.

REFERENCES

Arp H. C., Madore B. F., 1987, A Catalogue of Southern Peculiar Galaxies and Associations. Cambridge Univ. Press, Cambridge
Barnes J. E., 1988, ApJ, 331, 699
Bernlöhr K., 1993, A&A, 270, 20
Beswick R. J., Pedlar A., Clemens M. S., Alexander P., 2003, MNRAS, 346, 424
Brassington N. J., Read A. M., Ponman T. J. 2005, MNRAS, submitted
Colbert E., Heckman T., Ptak A., Strickland D., 2004, ApJ, 602, 231
Condon J. J., Condon M. E., Gisler G., Puschell J. J., 1982, ApJ, 252, 102
Condon J. J., Helou G., Sanders D. B., Soifer B. T., 1990, ApJS, 73, 359
Crawford D. F., Jauncey D. L., Murdoch H. S., 1970, ApJ, 162, 405
Devereux N. A., Eales S. A., 1989, ApJ, 340, 708
Fabbiano G., Zezas A., Murray S. S., 2001, ApJ, 554, 1035
Hibbard J. E., van Gorkom J. H., 1996, AJ, 111, 655
Read A. M., 2003, MNRAS, 342, 715
Read A. M., Ponman T. J., 1995, MNRAS, 276, 1327
Read A. M., Ponman T. J., 1998, MNRAS, 297, 143 (RP98)
Read A. M., Ponman T. J., Strickland D. K., 1997, MNRAS, 286, 626
Roberts T. P., Warwick R. S., Ward M. J., Murray S. S., 2002, MNRAS, 337, 677
Rosati P. et al., 2002, ApJ, 566, 667
Sanders D. B., Scoville N. Z., Sargent A. I., Soifer B. T., 1988, ApJ, 324, L55
Stanford S. A., 1991, ApJ, 381, 409
Stanford S. A., Balcells M., 1990, ApJ, 355, 59
Stanford S. A., Balcells M., 1991, ApJ, 370, 118
Stevens I. R., Read A. M., Bravo-Guerrero J., 2003, MNRAS, 343, L47
Stockton A., Bertola F., 1980, ApJ, 235, 37
Strickland D. K., Heckman T. M., Weaver K. A., Hoopes C. G., Dahlem M., 2002, ApJ, 568, 689
Swartz A. S., Ghosh K. K., Tennant A. F., Wu K., 2004, ApJS, 154, 519
Toomre A., 1977, in Tinsley B. M., Larson R. B., eds, Evolution of Galaxies and Stellar Populations. Yale University Observatory, New Haven, p. 401
Toomre A., Toomre J., 1972, ApJ, 178, 623
Tovmasyan H. M., Sramek R. A., 1976, Astrofizika, 12, 21
Tully R. B., 1988, Nearby Galaxies Catalogue. Cambridge Univ. Press, Cambridge
Yun M. S., Hibbard J. E., 2001, ApJ, 550, 104
Zezas A., Fabbiano G., 2002, ApJ, 577, 726

This paper has been typeset from a TEX/LATEX file prepared by the author.